coatings

MDPI

Article

The Influence of Niobium and Zirconium Addition on the Structural and Mechanical Properties of Yttrium Nitride: A First-Principles Study

Adel Bandar Alruqi

Department of Physics, Faculty of Science, King Abdulaziz University, Jeddah 21589, Saudi Arabia; aalruqi@kau.edu.sa

Abstract: Yttrium nitride (YN) is a hard and refractory material with a high melting point. It is a semiconductor that has been investigated for its potential applications in the field of semiconductor technology, including as a material for electronic devices. It is also of interest for its optical properties and its potential for use in optoelectronics. However, investigating its mechanical properties for a possible application in optical coatings has not been completed. This study involved the exploration of the mechanical properties of YN alloyed with niobium (Nb) and zirconium (Zr) for possible application in optical coatings using a first-principles approach. The result showed that the addition of Nb and Zr into the YN matrix had a profound effect on the mechanical properties of the modeled structures, with the Y-N-Nb (CYN_5) sample having the best mechanical properties. The bulk modulus was the most affected, with an increase of 26.48%, while the Vickers hardness had the smallest increase of 6.128% compared with those of pure YN. The modeled structures were thus found to be ideal alternative materials for optical coatings due to their improved mechanical properties.

Keywords: optical coatings; mechanical properties of optical coatings; mechanical properties of niobium compounds; mechanical properties of zirconium compounds; yttrium nitride alloys

Citation: Alruqi, A.B. The Influence of Niobium and Zirconium Addition on the Structural and Mechanical Properties of Yttrium Nitride: A First-Principles Study. *Coatings* **2023**, *13*, 2078. https://doi.org/10.3390/coatings13122078

Academic Editor: Alicia de Andrés

Received: 14 November 2023
Revised: 5 December 2023
Accepted: 9 December 2023
Published: 13 December 2023

1. Introduction

Yttrium nitride (YN) is a semiconductor composed of yttrium (Y) and nitrogen (N), and it belongs to the larger category of nitride compounds [1]. It is currently used in a wide range of applications. Silicon nitride powders are coated uniformly with yttria and yttria–alumina precursors using YN in microencapsulation procedures [2]. In metal/semiconductor superlattices for thermoelectric applications, YN is a semiconductor that shows great promise [3]. Moreover, YN is a good electrical conductor, making it appropriate for use in micro- and optoelectronics [4].

To improve the electrical conductivity in integrated circuits and other electronic devices, YN is used as a conductive layer in thin-film coatings [5,6]. The high Vickers hardness of YN at 22.28 GPa [4] implies that it possesses excellent hardness and wear resistance and has the potential to coat and shield underlying materials from abrasion and wear. For cutting tools and wear-resistant applications, this is useful in prolonging the lifespan and durability of the coated components. YN can be used in decorative coatings and as a more affordable option to gold coatings, thanks to its good reflection and color. Due to its corrosion resistance, it can be used as a protective coating in settings where exposure to corrosive materials is a problem [2,7]. YN has been explored both in 3D and 2D for coating applications, where the 2D structures have been found to possess unique properties [8].

Coating materials should have a number of desirable mechanical properties, including firmly adhering to the substrate in order to prevent delamination or peeling, especially under mechanical stress or temperature fluctuations [9]. The coating should also be hard to ensure a longer lifespan and to maintain the optical performance over time, such as

high transparency since it is resistant to scratches, abrasion, and wear [10,11]. To accommodate stress, strain, and thermal expansion differences between the coating and substrate without cracking or delamination, coatings should have a certain degree of elasticity and flexibility. Cleaning agents or contact with other surfaces should not significantly degrade the coating's optical properties. The coatings should also have the capacity to withstand crack propagation, which is essential to avoid damage from mechanical stresses or impacts. Moreover, the coatings should have the ability to endure wear over time, especially in situations where the coated surface may be subjected to repetitive friction or contact, as well as sustaining compression pressures without deforming or failing, which is crucial in applications where pressure is applied to the coating [12].

Despite the desirable properties mentioned, YN faces several challenges as an optical coating material. Firstly, it is not chemically inert since it has a high heat solution of 11.6 kcal/mol [6]. Thus, it cannot effectively resist reactions with many chemicals and gases. High inertness is ideal for ensuring the stability of the coating and making it suitable for use in various chemical environments. Secondly, Y is a relatively rare and expensive element [13]. Consequently, its cost and availability can be limiting factors in the widespread use of YN for coating applications. Although YN possesses good elastic properties such as a high bulk modulus for better resistance to compression, its mechanical properties still need modifications to make them better.

In optical coatings, maintaining a certain level of hardness and rigidity is important to ensure that the coating remains intact and does not undergo plastic deformation. Plastic deformation can introduce unwanted changes in the coating's structure and optical properties, leading to loss of performance or functionality. In this study, I performed ab initio mechanical characterization of YN alloyed with niobium (Nb) and zirconium (Zr) with the aim of improving those properties for possible application in optical coatings. The choice of the two materials (Nb and Zr) was informed by the relative abundance of Zr, as well as their low-toxic nature [14,15]. Moreover, Zr is known for its resistance to corrosion and heat, and it is currently being used in various industries, including nuclear power, aerospace, and the production of high-temperature alloys [16].

2. Materials and Methods

The starting structure (YN) was obtained from the crystallographic open database [17]. The cell was a simple cube, with an Fm3m space group, number 225 (Figure 1), and a lattice constant of 4.894 Å. The Y-N bond was found to be 2.447 Å (Figure 1). The original structure consisted of 8 atoms: 4 of Y and 4 of N. Upon creation of $2 \times 2 \times 2$ supercells (Figure 2a) containing 64 atoms (32 of Y and 32 of N), the structures were alloyed by replacing some of the Y atoms with those of Nb and Zr, as shown in Table 1. The alloyed structures are shown in Figure 2, which shows only a representation of one structure in each category, as presented in Table 1. It is worth noting that the number of N atoms was kept constant at 32 throughout, and only those of Y were substituted with those of Nb and Zr. The samples were given sample identities, as shown in Table 1. Co-alloying was also performed, where both Nb and Zr atoms were incorporated into the YN structure. For the Y-N-Nb-Zr samples, the number of Y atoms was kept constant at 12, and the number of atoms of Nb and Zr was varied, as shown (Table 1).

The modeling of the structures was performed using the SOD (site occupation disorder) algorithm, upon which the structures that produced the least total energies were selected for further analysis. The SOD code ensured that the modeled structures remained cubic, with the same space group as that of the original YN structure. The optimization of the modeled structures was performed according to the procedure found in the work by Alruqi and Ongwen [18]. The kinetic energy cut-off and the k_point meshes were taken as 50 Ry and $5 \times 5 \times 5$, respectively.

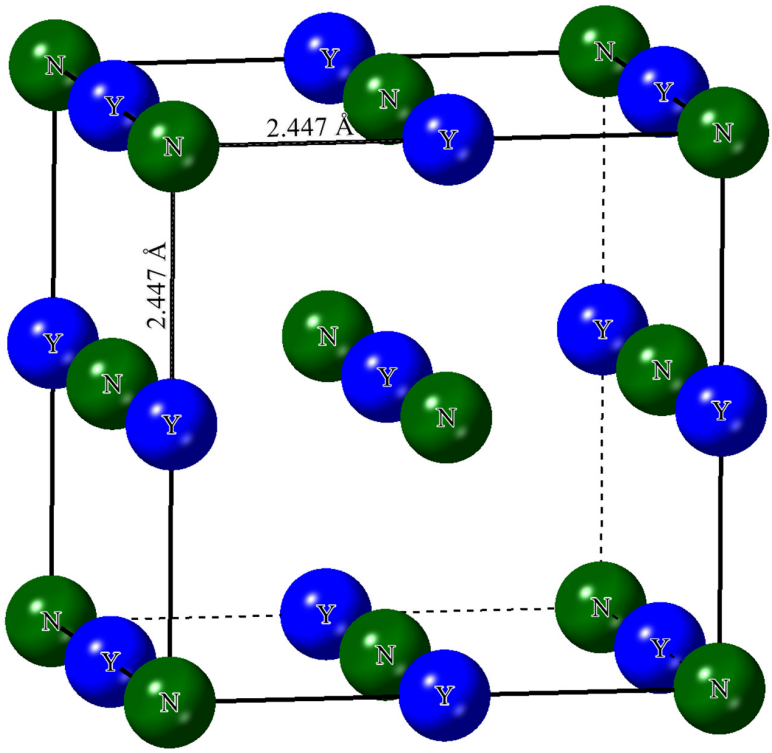

Figure 1. The 3D structure of a yttrium nitride cell.

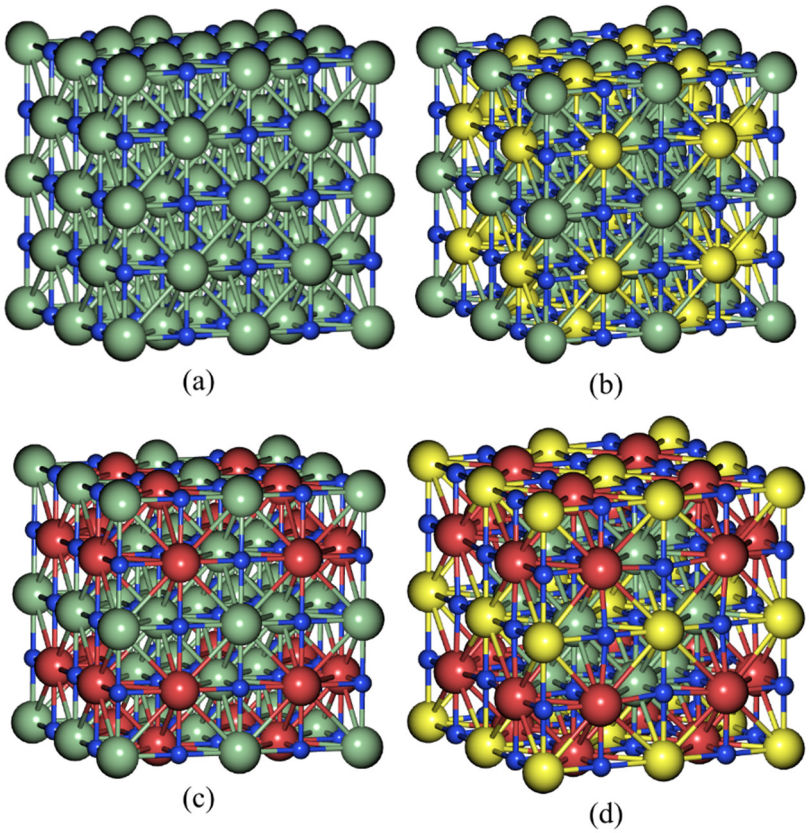

Figure 2. The 3D supercells of the alloyed samples: (**a**) YN (sample CY), (**b**) Y-N-Nb (sample CYN_3), (**c**) Y-N-Zr (sample CYZ_3), and (**d**) Y-N-Nb-Zr (sample CYNZ_2). The green spheres represent yttrium atoms, the blue spheres represent nitrogen atoms, the yellow spheres represent niobium atoms, and the red spheres represent zirconium atoms.

Table 1. The number of atoms of Y, N, Nb, and Zr in the Y-N-Nb, Y-N-Zr, and Y-N-Nb-Zr supercells.

	Sample	Yttrium	Nitrogen	Niobium	Zirconium
	CY	32	32	0	0
Y-N-Nb	CYN_1	28	32	4	0
	CYN_2	24	32	8	0
	CYN_3	20	32	12	0
	CYN_4	16	32	16	0
	CYN_5	12	32	20	0
Y-N-Zr	CYZ_1	28	32	0	4
	CYZ_2	24	32	0	8
	CYZ_3	20	32	0	12
	CYZ_4	16	32	0	16
	CYZ_5	12	32	0	20
Y-N-Nb-Zr	CYNZ_1	12	32	4	16
	CYNZ_2	12	32	8	12
	CYNZ_3	12	32	12	8
	CYNZ_4	12	32	16	4

All the calculations were performed using generalized gradient approximation within the Quantum Espresso algorithm. The calculation of the elastic constants (and hence, the mechanical properties) was determined using the stress–strain method from the work by Ongwen, Ogam, and Otunga [19]. Very small values of strains (±0.006) were applied to the crystals so as to ensure that resulting stresses remained within the linear regime of Hooke's law. The calculation of the Vickers hardness was performed using the Tian model, which is expressed as [20]:

$$H_V = 0.92n^{1.137}G^{0.708} \quad (1)$$

where $n = G/B$, where G is the shear modulus and B is the bulk modulus. Both the bulk and shear moduli used in this study were Hill's averages, which were obtained according to some previous works [21,22]. The mechanical stability of the structure was tested using the relationships:

$$c_{11} > 0,\ c_{44} > 0,\ c_{11} - c_{12} > 0,\ c_{11} - 2c_{12} > 0 \quad (2)$$

3. Results and Discussion

3.1. Structural Study

In many areas of research and engineering, the structural properties of a material are vital because they influence the material's behavior, functionality, and suitability for a certain use. These properties offer important insights into the behavior of materials under various loads, production conditions, and environments. They influence material performance, selection, design and engineering, failure analysis, and durability and longevity, among others [23,24]. The lattice constant of YN was found to be in very good accord with the literature values (Table 2). The lattice constant deviates from the experimental study by Du et al. [1] by 0.4082%, and from the computational study by Holec et al. [25] by 1.261%. The study by Du et al. obtained the rock salt structure of YN. The computed density of YN in this study is also in excellent accord with the result from the study by Holec et al. [25].

Table 2. The computed lattice parameters, density, and elastic stiffness constants of Y-N-Nb, Y-N-Zr, and Y-N-Nb-Zr.

Category	Sample	a (Å)	ρ (kg/m³)	c_{11} (GPa)	c_{12} (GPa)	c_{44} (GPa)
	CY	4.908 (4.88 [1]) (4.917 [4])	5788 (5750 [25])	312.0 (314.34 [4])	83.1 (81 [26])	123.6 (124 [26])
Y-N-Nb	CYN_1	4.824	6127	356.6	84.0	127.9
	CYN_2	4.766	6388	372.0	90.6	128.4
	CYN_3	4.715	6652	390.2	95.5	128.9
	CYN_4	4.649	6953	410.9	101.6	129.7
	CYN_5	4.592	7253	434.7	107.7	130.3
Y-N-Zr	CYZ_1	4.858	5985	340.6	85.3	128.2
	CYZ_2	4.816	6109	366.9	87.8	129.9
	CYZ_3	4.778	6327	389.1	90.3	131.6
	CYZ_4	4.738	6504	416.8	92.7	132.6
	CYZ_5	4.702	6673	447.3	95.1	134.1
Y-N-Nb-Zr	CYNZ_1	4.615	7125	441.9	99.6	100.0
	CYNZ_2	4.638	6981	442.7	99.7	110.1
	CYNZ_3	4.656	6908	443.7	99.8	118.7
	CYNZ_4	4.678	6792	445.1	99.9	128.6

Figure 3a clearly shows that the lattice constants of all the samples investigated in this study generally decrease upon the addition of the alloying elements (Nb and Zr). Nb led to a larger decrease in the lattice constant (Y-N-Nb) compared with Zr (Y-N-Zr). This can be attributed to the difference in the atomic radii of the three elements. Both Nb (198 pm) and Zr (206 pm) have smaller atomic radii compared with that of Y (212 pm). Thus, incorporating them into the YN matrix led to the shrinkage of the cell. Incorporating Nb led to a higher shrinkage since Nb has a smaller atomic radius compared with Zr. The addition of both Nb and Zr (Y-N-Nb-Zr) into the YN matrix led to a drastic drop in the lattice constant, after which the lattice constant increased consistently with the addition of Nb (and a decrease in Zr). The densities of the alloyed structures experienced an increase upon the addition of the two alloying elements (Figure 3b). This was expected since density and the lattice constant (volume) are inversely related. Going by the mechanical stability conditions in equation 2, it was concluded that all the materials investigated in this study are mechanically stable under ambient conditions.

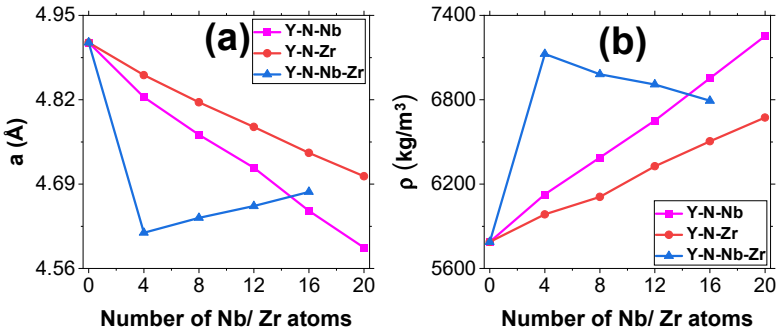

Figure 3. The variation in the computed lattice parameters and densities of the alloy samples as functions of the number of niobium/zirconium atoms. (**a**) Lattice parameter against the number of Nb/Zr atoms, and (**b**) density against the number of Nb/Zr atoms.

3.2. Mechanical Properties

In many disciplines, including engineering, materials science, and manufacturing, a material's mechanical properties are crucial. For the purpose of creating safe and effective structures, these properties offer vital information about how a material will respond to various loading scenarios. For structures to be efficient, safe, and reliable, their mechanical properties are essential. Mechanical properties such as Young's modulus and hardness are essential factors to take into account when choosing materials, designing products, and advancing industry and technology as a whole [27,28].

Table 2 also depicts the computed elastic stiffness constants c_{ij}. Only three stiffness constants (c_{11}, c_{12}, and c_{44}) are required for the calculation of the elastic constants of cubic crystals. As the table shows, the calculated stiffness constants are in excellent accord with the literature values. This is a result of the high accuracy that was used in the calculations, which was brought about by the large kinetic energy cut-off as well as the large k_point mesh. Going by the mechanical stability condition [29], I concluded that all the modeled structures in this study are mechanically stable under ambient conditions.

The elastic stiffness constant refers to the stiffness or elasticity of a material in a specific direction or for a particular mode of deformation. A larger value of the elastic stiffness constant indicates that the material is stiffer and more resistant to deformation in the specified direction. This is particularly significant in applications where rigidity and minimal deformation are crucial. As Table 2 shows, YN has a much larger value of the stiffness constant along the x-direction (c_{11}), implying that it can withstand greater loads or stresses along the x-direction before undergoing significant deformation or failure. This is important for ensuring the safety and reliability of structures and components, especially in applications where they experience substantial forces. The elastic stiffness constant c_{44} was observed to be larger than c_{12}, implying that the crystal is resistant to shear since c_{44} is related to shear [30].

Figure 4a shows the variation in the elastic stiffness constants of the samples with the number of Nb/Zr atoms. As the figure depicts, a consistent increase in c_{11} and c_{12} with the number of Nb/Zr is observed in all the samples, while the Y-N-Nb-Zr experienced a drop at Nb = 4 but then increased as the number of Nb increased. The increase in the stiffness constants can be attributed to the close-packed arrangement of the atoms in their structures. Elevated stiffness constant values in materials are noteworthy for multiple reasons since they greatly influence the material's mechanical properties and appropriateness for different uses. Characterizing a material's reaction to mechanical loads and deformations requires an understanding of the stiffness constants. The fact that materials with greater stiffness constants are less pliable and more rigid is the most obvious significance. They are more difficult to stretch or compress under a given force and resist deformation. This property is essential in applications that demand dimensional stability. Moreover, stiffer materials can bear more loads and pressures without experiencing undue deformation or failure. Because of this, they can be used in load-bearing parts in equipment, buildings, and other applications [31]. All the materials computed in this study therefore prove to be superior to YN since all have higher values of the elastic stiffness constants.

In Figure 4a, the curves for Y-N-Nb and Y-N-Zr for c_{11} are almost equal, while that for Y-N-Nb-Zr experiences a drastic rise at Nb = 4 and then rises slowly as the number of Nb atoms increases. For c_{12} (Figure 4b), the curve for Y-N-Nb rises higher than that for Y-N-Zr as the number of Nb/Zr increases, implying that there is closer packing between the atoms in the Y-N-Nb structure than the packing between the Y-N-Zr structure. The Y-N-Nb-Zr structure also experienced a drastic rise at Nb = 4 for c_{12} and then rose slowly as the number of Nb atoms increased (Figure 4b). In Figure 4c, the curves of c_{44} for both Y-N-Nb and Y-N-Zr are comparable, especially at low values of Nb/Zr. As the values of Nb/Zr increase, however, a deviation is observed. This implies that Zr contributes to higher values of the stiffness constant c_{44}. The drastic drop in c_{44} for Y-N-Nb-Zr at Nb = 4 indicates that the sample experiences the least stiffness at this value of Nb.

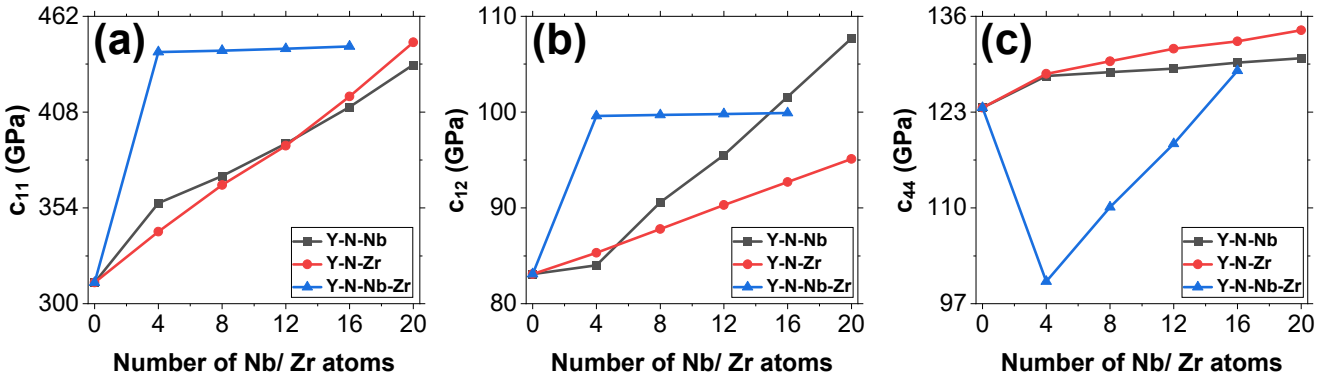

Figure 4. The variation of the computed elastic stiffness constants of the alloy samples as functions of the number of niobium/ zirconium atoms. (**a**) c_{11}, (**b**) c_{12}, and (**c**) c_{44}.

Table 3 displays the computed mechanical properties of YN and all the other materials simulated in this study. The mechanical properties of the pure YN (CY) are in excellent accord with the literature values, including the work by Yang and An [32], who used GGA-PBE in their work. The values of the mechanical properties of YN obtained in this study are higher than those of the common materials used in optical coatings.

Table 3. The computed mechanical properties of Y-N-Nb, Y-N-Zr, and Y-N-Nb-Zr.

Category	Sample	B(GPa)	G(GPa)	E(GPa)	H_V(GPa)
	CY	159.4 (159.2 [32])	119.9 (120.5 [32])	287.5 (289.2 [33])	20.56 (21.01 [32])
Y-N-Nb	CYN_1	174.9	131.3	314.8	21.78
	CYN_2	184.4	133.2	322.0	20.91
	CYN_3	193.7	136.0	330.6	20.40
	CYN_4	204.7	139.2	340.4	19.85
	CYN_5	216.8	142.7	351.0	19.34
Y-N-Zr	CYZ_1	170.4	128.0	307.1	21.45
	CYZ_2	180.8	133.7	321.8	21.62
	CYZ_3	189.9	138.7	334.2	21.73
	CYZ_4	200.7	143.7	348.0	21.78
	CYZ_5	212.5	149.6	363.4	21.82
Y-N-Nb-Zr	CYNZ_1	213.7	124.2	312.1	14.80
	CYNZ_2	214.0	131.6	327.6	16.66
	CYNZ_3	214.4	137.7	340.3	18.26
	CYNZ_4	215.0	144.7	354.5	20.11

For instance, magnesium fluoride (MgF_2) has a Young's modulus of 169.1 GPa, a shear modulus of 57.1 GPa, and a Vickers hardness of 4.41 GPa [34]. Silicon IV oxide (SiO_2), on the other hand, has a Vickers hardness of 11.5 GPa [35]. These figures show that YN has superior mechanical properties compared with those of both MgF_2 and SiO_2. Figure 5 shows the variation in the mechanical properties of the modeled samples with Nb/Zr. The bulk moduli of all the samples (Figure 5a) generally increase with an increase in the number of Nb and Zr atoms added. The material's resistance to compression under pressure is expressed in terms of its bulk modulus. A larger bulk modulus in the context of optical coatings can provide a number of noteworthy benefits. Optical coatings are frequently used in a variety of optical devices, including telescopes, microscopes, and

cameras, in order to enhance the performance of lenses and mirrors. The shape of the optical element is less likely to flex or distort when subjected to external forces when a material with a high bulk modulus is used in the coating because it is less prone to compression under pressure. As a result, there is less image distortion and better optical performance. Moreover, optical coatings exhibiting a high bulk modulus are characterized by greater resistance to mechanical deformation. Without experiencing major changes in their properties, they can tolerate external stresses like pressure, temperature swings, and vibrations. This is especially crucial for situations where optical components are exposed to challenging weather conditions [36,37]. All the materials investigated in this study turned out to have higher bulk moduli than those of YN Y-N-Nb (CYN_5), which had the highest bulk modulus of 216.8 GPa, representing a 26.48% increase from that of YN at 159.4 GPa. Thus, they are superior for use in optical coating applications. A consistent increase in the bulk modulus was observed with an increase in both Nb and Zr. The bulk modulus increased from 159.4 GPa (for YN) to 216.8, 212.5, and 215.0 GPa for Y-N-Nb, Y-N-Zr, and Y-N-Nb-Zr, respectively. This represents a maximum increase of 36.01% for CYN_5.

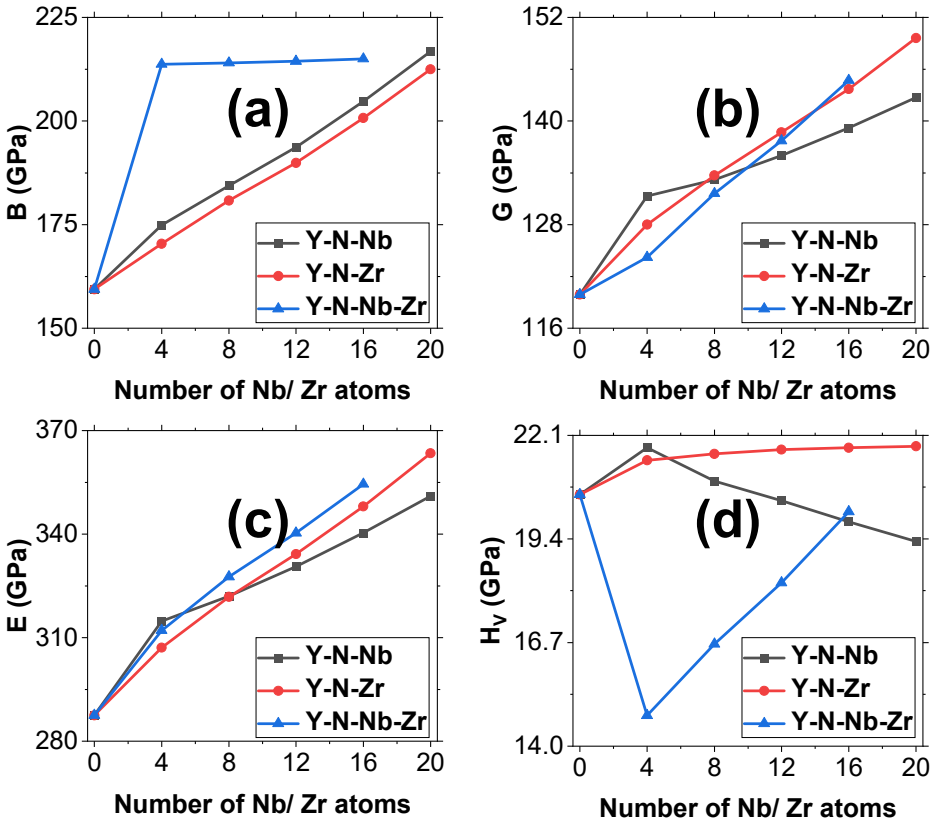

Figure 5. Variation in the computed mechanical properties of the alloy samples as functions of the number of niobium/zirconium atoms. (**a**) Bulk modulus, (**b**) Shear modulus, (**c**) Youngs modulus, and (**d**) Vickers hardness.

A material's resistance to deformation brought on by shear stress is determined by its shear modulus. A greater shear modulus in the context of optical coatings can offer a number of noteworthy benefits. Optical coatings, like interference coatings, are typically extremely thin layers of material. These coatings may experience shear forces when they are subjected to mechanical or environmental stress. Materials with a higher shear modulus are less likely to slip or shear under such stress, which lowers the possibility of deformation that could impair optical performance. Depending on the precise layer thickness and refractive index, optical coatings are engineered to have specific optical properties like reflectance, transmittance, or antireflection properties. These properties may alter due to

shear-induced deformation in the coating [38]. As Figure 5b shows, the shear moduli of all the samples increased consistently with an increase in the number of Nb/Zr atoms. The Y-N-Zr experienced the largest increase of 149.6 GPa (for sample CYZ_5), representing 24.77%, while CYN_5 recorded the least increase of 142.7 GPa. The high shear moduli of these materials imply higher mechanical stability and can aid in the coatings' ability to hold onto their intended characteristics over time, even in the face of mechanical stress and temperature changes.

When a material is exposed to a tensile or compressive force, its stiffness or resistance to elastic deformation is measured by its Young's modulus. A higher Young's modulus can have important implications for optical coatings for a number of reasons, including reduced deformation, improved resistance to mechanical stress, and enhanced optical performance. In order to retain their optical properties, optical coatings (which are frequently applied as thin layers on optical surfaces) must keep their thickness and shape. When subjected to mechanical stress, a material with a high Young's modulus is less likely to experience significant elastic deformation, which could result in slight alterations to the coating's thickness and shape. This is required in order to sustain optical performance. Moreover, mechanical stresses from handling, mounting, and temperature-induced expansion and contraction occur in optical systems. A greater resistance to these stresses means that a coating with a higher Young's modulus is less likely to deform, delaminate, or sustain damage. As a result, the optical system becomes stronger [39,40]. As Figure 5c shows, there is a consistent increase in Young's moduli with an increase in the number of Nb/Zr atoms. The Y-N-Nb samples (sample CYN_5) recorded the highest value of Young's modulus at 363.4 GPa, which was 26.4% higher than that of YN at 287.5 GPa. CYN_5 therefore provides greater performance of the optical coatings such as reflectivity or transmittance, as the coating's structure remains intact under stress. This stability is crucial for maintaining consistent optical performance.

The ability of a material to withstand permanent deformation when subjected to an applied load is gauged by its hardness. The ease of cleaning and maintenance of a coating can be influenced by its mechanical durability and hardness. Softer coatings might be more prone to scratches during cleaning, which, over time, could change the coating's optical properties. A greater Vickers hardness is important in the context of optical coatings for a number of reasons including scratch resistance, durability, improved longevity, and resistance to abrasion. Scratching can deteriorate optical coatings, lowering their optical performance. Coatings with a higher Vickers hardness are less likely to scratch, thus protecting the coated optical elements from harm caused by handling, cleaning, or unintentional contact. Moreover, a greater wear resistance is typically indicated by a higher hardness, which can prolong the life of optical coatings. Extended-life coatings require less replacement or maintenance, which lowers costs and downtime and prolongs their integrity [41,42]. Figure 5d shows that the Vickers hardness of the materials investigated did not exhibit a specific trend. The Vickers hardness of Y-N-Zr increased consistently with increase in the number of Zr atoms, and that of Y-N-Nb increased slightly at Nb = 4 before dropping consistently. The Vickers hardness of Y-N-Nb-Zr experienced a drastic drop at Nb = 4 and then rose steadily thereafter. The highest Vickers hardness was witnessed for Y-N-Nb (CYN_5) at 6.128% higher than that of YN. The computed Vickers hardness obtained in this work shows that all the samples are much harder than common coating materials such as MgF_2 and SiO_2. They are thus better than common coating materials in resisting abrasion, protecting the underlying optical elements from damage, and maintaining optical performance. Moreover, they can better withstand cleaning processes, such as wiping or ultrasonic cleaning, without sustaining damage, ensuring that the coatings remain free from debris or contamination.

4. Conclusions

This study successfully investigated the structural and mechanical properties of Y-N-Nb, Y-N-Zr, and Y-N-Nb-Zr for optical coatings. The computed lattice constant of YN was found to be in excellent accord with the literature values. Both the alloying elements had a profound effect on the lattice constant of YN. The lattice constant decreased upon the addition of the two alloying elements, with Nb causing a larger decrease than Zr. The densities of the alloyed structures increased with the addition of the alloying elements. The calculated elastic stiffness constants of the samples showed that c_{11} and c_{12} increased consistently with the number of Nb/Zr atoms, while for c_{44}, Y-N-Nb-Zr experienced a drop at Nb = 4 before rising again with a further increase in the number of Nb atoms. The mechanical properties of the alloyed samples were found to be superior to those of pure YN and common coating materials such as MgF_2 and SiO_2, with Y-N-Nb (CYN_5) giving the best overall values. The bulk modulus increased by 26.48%, the shear modulus increased by 24.77%, Young's modulus increased by 26.4%, and the Vickers hardness recorded the smallest increase of 6.128% compared with those of pure YN. Although the results obtained in this study are very good for optical coatings, this study was purely computational. Therefore, an experimental investigation needs to be conducted in order to synthesize and verify the values of the properties obtained in this study. Moreover, since the performance of optical coatings heavily relies on the optical and mechanical properties of the coating materials, these properties need to be investigated for the modeled structures.

Funding: This research work was funded by Institutional Fund Projects under grant no. (IFPIP:1545-130-1443). The author gratefully acknowledges the technical and financial support provided by the Ministry of Education and King Abdulaziz University, DSR, Jeddah, Saudi Arabia.

Institutional Review Board Statement: Not applicable.

Informed Consent Statement: Not applicable.

Data Availability Statement: Data are contained within the article.

Conflicts of Interest: The author declares no conflict of interest.

References

1. Du, L.; Edgar, J.H.; Peascoe-Meisner, R.A.; Gong, Y.; Bakalova, S.; Kuball, M. Sublimation crystal growth of yttrium nitride. *J. Cryst. Growth* **2010**, *312*, 2896–2903. [CrossRef]
2. Garg, A.; Jonghe, L. Microencapsulation of silicon nitride particles with yttria and yttria-alumina precursors. *J. Mater.* **1990**, *5*, 136–142. [CrossRef]
3. Saha, B.; Sands, T.; Waghmare, U. Electronic structure, vibrational spectrum, and thermal properties of yttrium nitride: A first-principles study. *J. Appl. Phys.* **2011**, *109*, 073720. [CrossRef]
4. Cherchab, Y.; Mir, A.; González-Hernández, R.; Talbi, K.; Bennadji, A. The role of the scandium element concentration in the YN matrix: Ab initio study of structural, electronic, mechanical and thermal properties. *Int. J. Quantum Chem.* **2021**, *121*, e26791. [CrossRef]
5. Cruz, W.; Díaz, J.; Mancera, L.; Takeuchi, N.; Soto, G. Yttrium nitride thin films grown by reactive laser ablation. *J. Phys. Chem. Solids* **2003**, *64*, 2273–2279. [CrossRef]
6. Carlson, O.; Lichtenberg, R.; Warner, J. Solid solubilities of oxygen, carbon and nitrogen in yttrium. *J. Less Common Met.* **1974**, *35*, 275–284. [CrossRef]
7. Beck, U.; Reiners, G.; Kopacz, U.; Jehn, H. Decorative hard coatings: Interdependence of optical, stoichiometric and structural properties. *Surf. Coat. Technol.* **1993**, *60*, 389–395. [CrossRef]
8. Zheng, F.; Xiao, X.; Xie, J.; Zhou, L.; Li, Y.; Dong, H. Structures, properties and applications of two-dimensional metal nitrides: From nitride MXene to other metal nitrides. *2D Mater.* **2022**, *9*, 022001. [CrossRef]
9. Mehdinia, A.; Aziz-Zanjani, M. Recent advances in nanomaterials utilized in fiber coatings for solid-phase microextraction. *Trends Anal. Chem.* **2013**, *42*, 205–215. [CrossRef]
10. Fischer-Cripps, A. Chapter 14—Mechanical characterizations of surfaces and coatings. In *Materials Surface Processing by Directed Energy Techniques*; European Materials Research Society Series; Pauleau, Y., Ed.; Elsevier: Amsterdam, The Netherlands, 2006; pp. 475–499. [CrossRef]

11. Wu, B.; Yuan, A.; Xiao, Y.; Wang, Y.; Lei, J. Study on a polyacrylate-based waterborne coating: Facile preparation, convenient self-healing behavior and photoluminescence properties. *J. Mater. Chem. C* **2020**, *8*, 12638–12647. [CrossRef]
12. Wang, Z.; Wang, K.; Huang, H.; Cui, X.; Shi, X.; Ma, X.; Li, B.; Zhang, Z.; Tang, X.; Chiang, M. Bioinspired wear-resistant and ultradurable functional gradient coatings. *Small* **2018**, *14*, 1802717. [CrossRef]
13. Tolstov, A.; Pokhilenko, N.; Samsonov, N. New opportunities for producing rare earth elements one of the arctic raw material source. *J. Sib. Fed. Univ.* **2017**, *10*, 125–138. [CrossRef]
14. Galletti, A.; Pampaloni, G. Niobium complexes as catalytic precursors for the polymerization of olefins. *Coord. Chem. Rev.* **2010**, *254*, 525–536. [CrossRef]
15. Ghosh, S.; Sharma, A.; Talukder, G. Zirconium: An abnormal trace element in biology. *Biol. Trace Elem. Res.* **1992**, *35*, 247–271. [CrossRef] [PubMed]
16. Bird, K.; Richardson, K. Zirconium for superior corrosion resistance. *Adv. Mater. Process.* **1997**, *151*, 19–20.
17. Available online: http://crystallography.net/cod/result.php (accessed on 28 November 2023).
18. Alruqi, A.B.; Ongwen, N.O. A comparative thermodynamic study of AlF_3, ScF_3, $Al_{0.5}Sc_{0.5}F_3$, and $In_{0.5}Sc_{0.5}F_3$ for optical coatings: A computational study. *Coatings* **2023**, *13*, 1840. [CrossRef]
19. Ongwen, N.O.; Ogam, E.; Otunga, H.O. Ab initio study of elastic properties of orthorhombic cadmium stannate as a substrate for the manufacture of MEMS devices. Mater. *Today Commun.* **2021**, *26*, 101822. [CrossRef]
20. Avery, P.; Wang, X.; Oses, C.; Gossett, E.; Proserpio, D.M.; Toher, C.; Curtarolo, S.; Zurek, E. Predicting superhard materials via a machine learning informed evolutionary structure search. *Comput. Mater.* **2019**, *5*, 89. [CrossRef]
21. Wang, J.; Chen, S.; Yang, Y.; Yu, Y.; Dong, H.; Li, Y. Bulk structure of Si_2BN predicted by computational approaches. *Diam. Relat. Mater.* **2022**, *130*, 109530. [CrossRef]
22. Matar, S.F.; Solozhenko, V.L. New superhard tetragonal BCN from crystal chemistry and first principles. *Materialia* **2022**, *26*, 101581. [CrossRef]
23. Rajasekaran, G.; Narayanan, P.; Parashar, A. Effect of point and line defects on mechanical and thermal properties of graphene: A review. *Crit. Rev. Solid State* **2016**, *41*, 47–71. [CrossRef]
24. Miskin, M.; Khaira, G.; Pablo, J.; Jaeger, H. Turning statistical physics models into materials design engines. *Proc. Natl. Acad. Sci. USA* **2015**, *113*, 34–39. [CrossRef] [PubMed]
25. Holec, D.; Friák, M.; Neugebauer, J.; Mayrhofer, P.H. Trends in the elastic response of binary early transition metal nitrides. *Phys. Rev. B* **2012**, *85*, 064101. [CrossRef]
26. Miháliková, I.; Friák, M.; Jirásková, Y.; Holec, D.; Koutná, N.; Šob, M. Impact of nano-scale distribution of atoms on electronic and magnetic properties of phases in Fe-Al nanocomposites: An ab initio study. *Nanomaterials* **2018**, *8*, 1059. [CrossRef]
27. Vo, T.; Reeder, B.; Damone, A.; Newell, P. Effect of domain size, boundary, and loading conditions on mechanical properties of amorphous silica: A reactive molecular dynamics study. *Nanomaterials* **2020**, *10*, 54. [CrossRef]
28. Safont, G. Mechanical properties of materials. In *Introduction to Contact Mechanics*; Mechanical Engineering Series; Springer: Boston, MA, USA, 2007. [CrossRef]
29. Pius, K.K.; Ongwen, N.O.; Mageto, M.; Odari, V.; Gaitho, F.M. Mechanical properties of Al–Mg–Si alloys (6xxx Series): A DFT-based study. *Alloys* **2023**, *2*, 213–226. [CrossRef]
30. Smirnova, E.; Sotnikov, A.; Ktitorov, S.; Schmidt, H. Low temperature acoustic characterization of PMN single crystal. *J. Appl. Phys.* **2017**, *122*, 084103. [CrossRef]
31. Nazir, M.; Mahmood, T.; Zafar, A.; Akhtar, N.; Hussain, T.; Saeed, M.; Aleem, F.; Saeed, A.; Raza, J.; Cao, C. Electronic, optical and elastic properties of cubic zirconia (c-ZrO_2) under pressure: A DFT study. *Phys. B Condens.* **2021**, *604*, 412462. [CrossRef]
32. Yang, J.W.; An, L. Ab initio calculation of the electronic, mechanical, and thermodynamic properties of yttrium nitride with the rock salt structure. *Phys. Status Solidi B* **2014**, *251*, 792–802. [CrossRef]
33. Hao, A.; Yang, X.; Wang, X.; Yu, R.; Liu, R. First-principles investigations on electronic and elastic properties of YX (X = N, P, As and Sb) under high pressure. *Comput. Mater. Sci.* **2010**, *48*, 59–64. [CrossRef]
34. Available online: https://www.lakeshore.com/docs/default-source/default-document-library/magnesium-fluoride-mgf2-transmission-curve-datasheet.pdf?sfvrsn=8be6c56a_2 (accessed on 28 November 2023).
35. Suprapedi; Muljadi; Sardjono, P. The characterization of ceramic alumina prepared by using additive glass beads. *IOP Conf. Ser. Mater. Sci. Eng.* **2017**, *299*, 012043. [CrossRef]
36. Maidanik, G.; Maga, L. Analytical evaluation in the design of a coating. *J. Sound Vib.* **2008**, *309*, 150–166. [CrossRef]
37. Reddy, R.; Ahammed, Y.; Gopal, K.; Azeem, P.; Rao, T.; Reddy, P. Optical electronegativity, bulk modulus and electronic polarizability of materials. *Opt. Mater.* **2000**, *14*, 355–358. [CrossRef]
38. Shiue, S. Design of the interfacial shear strength between the glass fiber and primary coating in double-coated optical fibers. *J. Lightwave Technol.* **1999**, *17*, 1657–1661. [CrossRef]
39. Chen, S.; Shiue, S. Theoretical analysis of the interfacial-shear-stress induced delamination of polymeric coatings from the glass fibers in double-coated optical fibers during temperature cycling. *Opt. Fiber Technol.* **2006**, *12*, 268–275. [CrossRef]
40. Shen, T.; Shiue, S. Long-term thermally interfacial-shear-stress-induced delamination of polymeric coatings from glass fibers in double-coated optical fibers. *Opt. Eng.* **2003**, *42*, 1456–1459. [CrossRef]

41. Ali, M.; Islam, A.; Hossain, M.; Parvin, F. Phase stability, elastic, electronic, thermal and optical properties of $Ti_3Al_{1-x}Si_xC_2$ ($0 \leq x \leq 1$): First principles study. *Phys. B Condens. Matter* **2012**, *407*, 4221–4228. [CrossRef]
42. Guenther, K.; Bangert, H.; Kaminitschek, A.; Wagendristel, A. Ultra-microhardness testing of optical coatings. In *Third Topical Meeting on Optical Interference Coatings*; Technical Digest Series; Paper WA5; Optica Publishing Group: Monterey, CA, USA, 1984. [CrossRef]